1

Chapter 1

General introduction

1. General Introduction

Magnetic Resonance Imaging (MRI) and Magnetic Resonance Spectroscopy (MRS) are both important non-invasive tools in the field of biomedical research. The most common application is in the brain: however, adaptation of these MR techniques make them applicable to many other tissues and organs. One of these fields is musculoskeletal imaging where many different techniques are available to map various characteristics of healthy and diseased skeletal muscle. An important development in this field is the switch from qualitative visual assessment to quantitative measurements of tissue properties, which can be used to map the course of a disease, to evaluate potential therapeutic effects, and to investigate the effects of potential confounding factors on interpretation. One of the most common applications is in muscular dystrophies.

1.1 Skeletal muscle

Skeletal muscle is a highly ordered structure surrounded by connective tissue called the epimysium. The epimysium encloses the whole muscle and protects it from friction against other muscles and bones. A muscle consists of multiple fascicles, each surrounded by the perimysium and containing multiple fibers, which are in turn enclosed by the endomysium. All these connective tissue layers are interconnected and play an important role in force transmission. Small blood vessels and motor axons cross the perimysial space to make connections with muscle fibers. An individual muscle fiber is filled with sarcoplasm in which the myofibrils, ribosomes and mitochondria are located. In the myofibril, protein filaments (myofilaments) are organized in repeating units called sarcomeres. A sarcomere includes actin and myosin, contractile proteins which are essential for the generation of a muscle contraction. In addition to these contractile proteins, there is a wide variety of structural proteins in the sarcomere such as titin, nebulin and dystrophin, whose function is to maintain the architecture of the sarcomere. These organized repeating units are surrounded by the endoplasmic reticulum (Figure. 1.1). The endoplasmic reticulum stores calcium ions which are released when an action potential arrives at the T-tubulus. The rapid release of calcium ions activates the myofilaments that work together to generate force. The force developed in an individual muscle cell needs to be transferred to the musculoskeletal system in order to facilitate movement. The interconnection of all the connective tissue layers ensures that force is transferred to the tendon which is connected to the skeleton and finally results in movement.

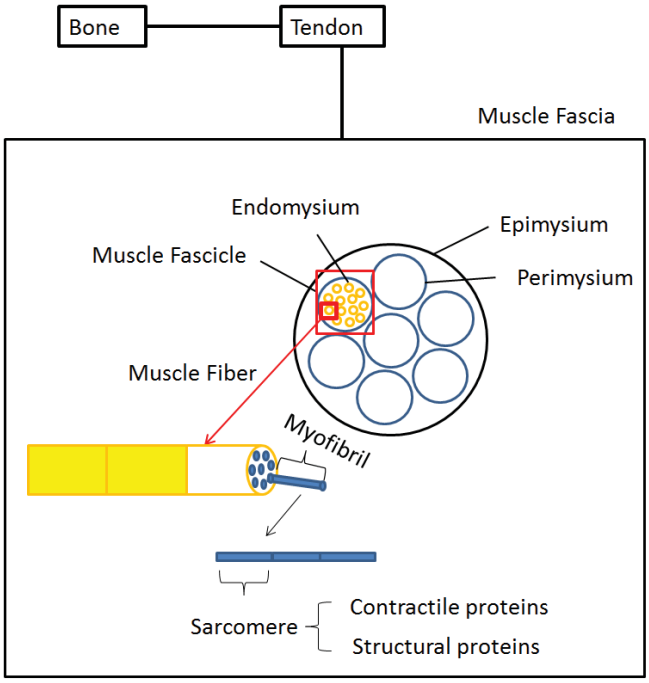

Figure 1. A schematic overview of skeletal muscle showing the arrangement of the various components.

1.2 Duchenne Muscular Dystrophy

Clinical phenotype

Duchenne Muscular Dystrophy (DMD) is the most common neuromuscular disorder, with an incidence of 1 in 3500 newborn boys. [1] It is an X-linked disease caused by a mutation in the *DMD* gene which codes for the protein dystrophin within the muscle cell. [2] The disease is characterized by progressive muscle damage, weakness and functional impairment. In DMD patients, the first symptoms often become apparent between the ages of 2 and 4 years old and consist of walking abnormalities, difficulties in climbing stairs, rising from the floor and running. [3] Many patients show pseudo-hypertrophy of the muscles, most notably in the calf muscles. The progressive loss of muscle strength results in wheelchair dependence in their early teens, after which upper limb function starts to decrease and frequently, scoliosis occurs. [4-6] In the late teens, patients develop respiratory impairments and need assisted ventilation.[7,8] In all DMD patients the heart muscle also becomes affected with age and mainly results in dilated cardiomyopathy.[9] Some patients suffer from learning and behavioral disabilities and the Intelligence Quotient (IQ) has been found to be one standard deviation below the general population.[10-12] Although life expectancy and quality of

life gradually increased due to treatment with corticosteroids, assisted ventilation and spinal fixation for severe scoliosis, most DMD patients die in their mid-thirties due to cardiac and respiratory failure. [13]

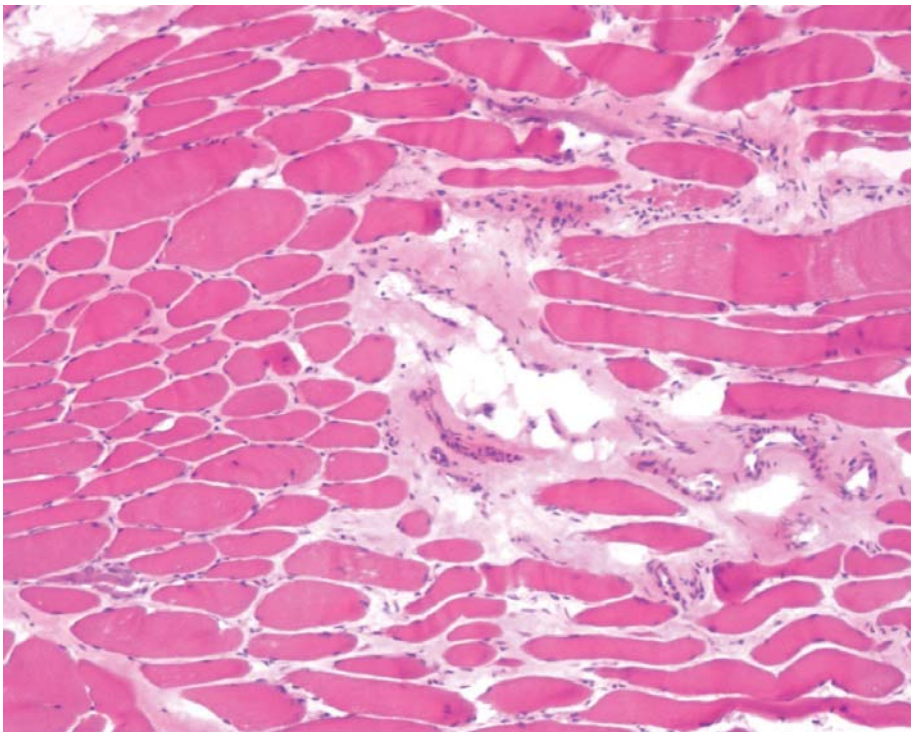

Figure 2. Cross-section of a muscle biopsy of the tibialis anterior muscle of a DMD patient showing the variations in fiber size, fibrosis, regeneration and degeneration of fibers, inflammatory cells and fat infiltration.

Muscle pathology

In muscle, dystrophin anchors the contractile apparatus to the muscle basement membrane via connections with the dystroglycoprotein complex.[14,15] Absence of dystrophin results in ongoing muscle damage, but the exact mechanism of how deficiency of dystrophin causes degeneration of muscle fibers is not fully understood. [16] Within muscle tissue different pathophysiological events take place, such as changes in energy metabolism, inflammation, fibrosis and fat replacement. These pathological hallmarks are clearly visible in muscle biopsies which contain an increased variation in fiber size, fibrotic and fatty tissue as well as groups of necrotic or degenerated fibers (Figure2). [17] The exact time course of these various processes is not fully understood, but it is thought that fiber necrosis induces a chronic inflammatory response that triggers fibrosis. At the same time, regeneration takes place through activation of

satellite cells.[4,18] Nonetheless, exhaustion of this regeneration capacity of the muscle eventually results in the replacement of muscle tissue by fat and connective tissue which is considered to be the end stage of the disease. [19] It is not completely clear whether the initial increase in muscle mass through hypertrophy is to compensate in part for the loss of force-generating capacity or should be considered an intrinsic aspect of this type of muscular dystrophy. [20,21]

1.3 Quantitative MR in skeletal muscle.

MR contrast

In MR the effect of two primary relaxation mechanisms on water protons is used to create image contrast, T_1 and T_2 relaxation. T_1 relaxation is the mechanism by which the longitudinal magnetization returns to its thermal equilibrium and reflects the energy transfer from spins to the environment, consisting of atoms and macromolecules. Each of these structures has its own characteristic tumbling rate (motion of the spin) which depends on the size and structure of the molecule and is driven by the thermal energy. The T_1 is shortest when the tumbling rate is almost equivalent to the Larmor frequency of the spin in the main magnetic field, both faster and slower tumbling rates are less efficient and result in longer T_1's. T_2 relaxation is the dephasing of the transverse magnetization and is determined by the interactions between spins in the tissue, which will lead to slight differences in resonance frequency. This difference in frequencies is measured by the dephasing of spins and generates T_2 contrast. By varying of sequence parameters, such as echo time (TE) and repetition time (TR), different image contrasts can be generated based on the T_1 and T_2 of the tissue.

MR in Skeletal muscle

Skeletal muscle has a short T_2 relaxation time, long T_1 relaxation time and high diffusivity of water protons. Consequently, application of MR techniques in skeletal muscle is challenging, as these tissues intrinsic MR properties all act to reduce the MR signal in a given sequence. These intrinsic tissue characteristics can change due to damage and disease, and as such can be a direct reflection of the disease. However, these pathology-related changes, for example muscle inflammation, metabolic alterations, or the replacement of muscle tissue by fat, can also act as confounders in the MR measurement. The recent switch from qualitative to quantitative assessment of skeletal muscle tissue properties with MR stresses the importance of high quality data, and the need to correct for such confounding effects. Acquisition of high quality data can naturally be achieved by using long measurement times. However, these long measurement times are generally experienced as uncomfortable and increase the risk of, for example, movement during the measurements which can

directly affect data-quality. In addition, a wide variety of MR-related parameters need to be assessed in order to be able to correct for any potential confounding factors, which is a time-consuming process. For newly-introduced techniques, it is generally unclear if there are any confounding factors and what, in the end, the effect might be on the measurements: the existence of confounding factors needs to be investigated to determine their effects on the final quantitative information from the scans.

Magnetic Resonance Imaging and Spectroscopy in DMD

Quantitative MR techniques have been frequently used to assess individual pathophysiological processes in Duchenne Muscular Dystrophy (DMD). [22] To start with, the replacement of muscle tissue by fat and connective tissue has been studied extensively. Both quantitative and semi-quantitative techniques showed variations in the extent and the rate of disease progression between different leg muscles.[20,23-29] In addition, quantitative techniques also showed that muscle fat fraction correlated well with disease progression and functional measures. Another MR measure which is often used in DMD, and is thought to reflect the inflammation component of the disease, is water T_2 relaxation times. Water T_2 values have shown to be elevated compared to healthy controls and to decrease with age and disease progression in DMD. [30-32] Moreover, water T_2 values have been shown to decrease towards more healthy values after three months of corticosteroid treatment. [33] Consequently, both muscle fat fraction and water T_2 values are frequently used as outcome measures in therapeutic evaluations (https://clinicaltrials.gov/search?cond=DMD+Therapy+MRI). Finally, changes in energy metabolism can be detected with phosphorous spectroscopy (^{31}P MRS). Elevated phosphodiesters levels, reduced phosphocreatine levels and a more alkaline intracellular tissue pH have been detected in DMD.[34-37] In addition, changes in energy metabolites have been found in relation to age, disease progression and functional measures. [37-41] So far the main focus of the field has been on quantifying individual pathophysiological processes in relation with function, disease progression, therapy and on detecting differences between individual muscles. However, to date, very little is known about how these individual pathophysiological processes relate to each other as well as to differences within an individual muscle.

Challenges in scanning of (young) children

Imaging studies in young pediatric populations remain relatively scarce due to the practical and technical challenges imposed during scanning of non-sedated subjects. Those challenges include motivation, alertness and cooperation of the child, but also anxiety caused by loud noise and the confined space of an MR scanner.

Various strategies have been proposed to improve a child's compliance during scanning without using sedation. [42] In the studies described in this thesis we used a mock scanner combined with a clear explanation of the procedure in appropriate terminology and a flexible approach based on the needs of the participant to improve the compliance. In addition to this, wearing their own metal-free clothing, bringing their own stuffed animal, and listening to their own music can result in a more familiar situation which improves the state of the patient. The presence of a parent, sibling or friend of the family in the MRI room can also put the child at ease. Alternatively, the presence of parents, sibling or guardians can also negatively influence the child which complicates the scanning procedure. During scanning, it is highly important to be aware of the state of the participant, as children sometimes do not express their feelings. Boredom, anxiety, discomfort and frustrations need to be detected and dealt with properly to ensure data quality: for example by using compliments, positive feedback and reminders about the essential things during scanning.

A number of MRI and MRS techniques applied in skeletal muscle will be discussed in more detail in the following section, as they are an essential part of this thesis. The discussion will focus on the basic characteristics of the method, confounders, data quality and factors which need to be considered during quantification.

1.4 Water fat imaging and ^{1}H MRS to assess muscle fat infiltration

One of the most common pathophysiological changes in damaged and diseased skeletal muscle is the progressive replacement of muscle tissue by fat. [43,44] [45,46] There are two main approaches used to assess muscle fat infiltration in skeletal muscle.

^{1}H MRS

The first approach is single voxel (SV) proton spectroscopy (^{1}H MRS) which is based on the difference in resonance frequency between water and fat protons. This technique measures the net equilibrium precessing magnetization of a desired nucleus, in this case protons, in a specific volume of interest, and depicts it as a function of their resonance frequency. This results in a frequency spectrum in which the resonances can be assigned to known functional groups, such as water and lipid (and also other macromolecules), and can be quantified. The total lipid signal in a typical ^{1}H spectrum consists of a number of spectral peaks at varying resonances and with varying amplitudes, while the water protons resonate at a single frequency (Figure 3). The lipid signal measured at clinical field strengths is represented by six fat peaks. It is dominated by lipid frequencies resonating between 0.5-2.75 ppm, and is often referred to as the aliphatic fat peak.[47] The lipid signal resonating at 5.3 ppm,

very close to the water signal, is called the olefinic fat peak. The apparent fat fraction can be derived from the integrated area of all the lipid signals and the water signal. One of the disadvantages of this method is that it only reflects a specific volume of interest. Therefore, it is less representative in heterogeneous tissue types, or in situations where one needs information from multiple muscles at once.

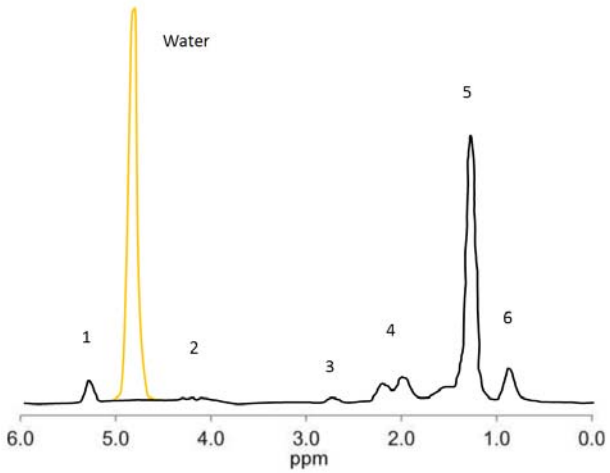

Figure 3. A proton MR spectrum at 3T. Water signal appears as a single peak at 4.7ppm (orange), whereas the fat signal is represented by six peaks (black), including the olefinic fat peak at 5.3 ppm (1), the peak at 4.1 ppm (2), the diacyl peak 2.7 ppm (3), the a-olefinic and a-carboxyl peak at 2.1 ppm (4), the dominant methylene peak at 1.3 ppm (5) and the methyl peak at 0.9 ppm (6).

Water Fat Imaging

The second approach is a quantitative imaging technique called Dixon, first introduced in 1984.[48] This method also allows separation of water and fat tissue based on the difference between the precessional frequencies of protons in water and fat. The conventional 2-point-DIXON method relies on the acquisition of two images with a gradient echo sequence, one in which water and fat are in-phase (IP) and one in which water and fat are out-of-phase (OP). Adding and subtracting these two images generates water and fat images, which combined can be used to quantitatively calculate an apparent fat fraction (Figure 4). One of the drawbacks of this method is that the reliability of the fat and water separation, by adding and subtracting images, is highly dependent on the magnetic field (B_o) inhomogeneities. This conventional method has been extended to the so-called 3-point-Dixon method which contains an additional third echo resulting in the ability to account for phase differences introduced by minor field inhomogeneities.[49] However, the situation described above is oversimplified, since it assumes a single resonance frequency

for water and fat, whereas the fat signal consists of a number of spectral peaks all contributing differently to the total fat signal. [47,50] The underlying algorithm of the 3-point Dixon can be modified to account for the individual fat spectral peaks.[51 52]

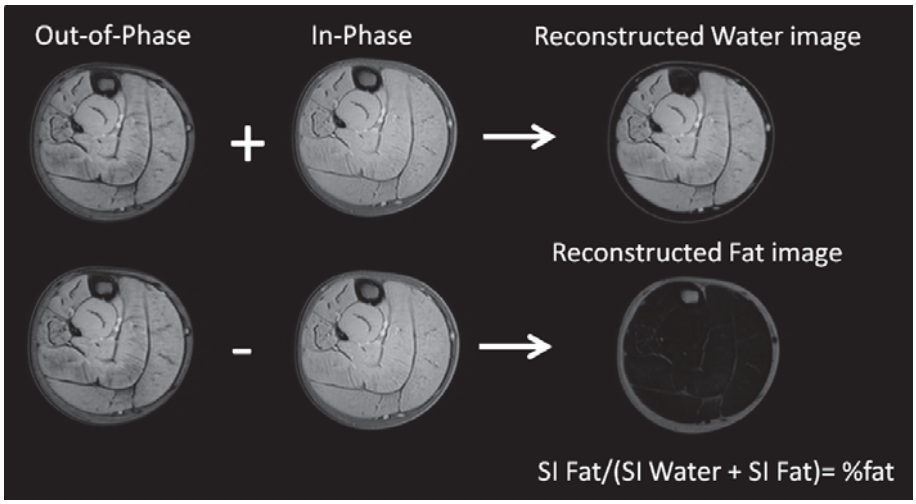

Figure 4. Axial in-phase (IP) and out-of-phase (OP) images and their reconstructed water and fat map of a right lower leg of a DMD patient. Note that the bright signal in the water images originates from muscle while in the fat images the bright signal is located in the subcutaneous fat.

The gradient echo 3-point Dixon method is used for all studies quantitatively assessing fat fraction in this thesis. A few factors will be discussed that need to be considered during the Dixon quantification process. First, the T_1 relaxation effect which could result in an overestimation of the fat fraction, due to a shorter T_1 of fat, as this difference in T_1 relaxation time between water and fat protons results in quicker relaxation of the fat signal within a short sequence TR.[53,54] For the data to be truly quantitative, this effect has to be minimized by using appropriate sequence parameters, for instance by using an optimized combination of a specific flip angle and TR. Secondly, the number of peaks taken into account in the reconstruction algorithm has a pronounced effect on the accuracy of the assessed fat fraction. Single peak models, solely aimed at the dominant methylene fat peak, responsible for 70% of the total fat signal, have shown to underestimate the total fat fraction compared to multi-peak models.[55,56] Another confounder is the T_2* relaxation effect, which originates from signal relaxation between echoes due to minor field inhomogeneities. [57] Despite the fact that this effect is small in tissues with no significant iron concentrations, this could result in an overestimation of fat fractions in low fat ranges. These effects can be accounted for in post-processing, where a minimum of three echoes is essential to generate a proper T_2* correction. [58]

1.5 (Water) T_2 relaxation time to assess inflammation and edema-like processes

The T_2 relaxation time is a tissue specific constant which reflects the interaction of a group of proton spins dephasing with respect to each other. The T_2 relaxation behavior should be mono-exponential in case of a single component, such as protons in water that reside in the same compartment. However, the transverse relaxation behavior of most biological tissues, including muscle, has shown to be multi-exponential. [59] Changes in T_2 are often associated with pathology, for example elevated water T_2 values in skeletal muscle are thought to reflect processes such as inflammation or edema. Elevated water T2 values are also found after exercise. By contrast, reduced water T_2 values in skeletal muscle have been associated with fibrosis. [60,61]

^{1}H MRS to assess water T_2

There are two main techniques used to quantitatively assess water T_2 relaxation time in skeletal muscle. First of all, SV ^{1}H MRS which measures the T_2 relaxation behavior of any tissue component independently of others, in this case water, and is *in-vivo* generally reflected by a mono-exponential fit. This MRS method with mono-exponential fit is assumed to be the gold standard and has been shown to be a robust and quantitative measure to assess water T_2 within a specific region of interest in both healthy and diseased tissue. [62-64] However, as mentioned before, this method can only generate information from one specific region of interest and is therefore not representative in heterogeneous tissue types.

Quantitative T_2 imaging to assess water T_2

The second approach is a Multi Spin Echo (MSE) acquisition, which is a quantitative imaging method that can cover a large region of interest (ROI) and contains information from multiple muscles at once. This approach is based on a simple Carr-Purcell-Meiboom-Gill sequence, where a 90-degree pulse is followed by a series of 180-degree pulses at multiple echo times, which allows assessment of the relaxation behavior of protons bound to various tissue components. The T_2 relaxation times of these tissue components can differ. For example, the T_2 relaxation time of fat protons is relatively long (> 90ms) compared to that of water (25-30ms). These two components together, when originating from the same tissue compartment, create a bi-exponential signal. However, the relaxation behavior of these two tissue components can still be approximated by a mono-exponential fit. [65,66] This combined relaxation behavior of protons in water and fat is then referred to as global T_2 values. In healthy skeletal muscle, global T_2 values and water T_2 values are almost equivalent, due to the only very minor contributions of the protons in fat. However, one of

the most common pathophysiological changes in damaged and diseased muscle is the replacement of muscle tissue by fat. Consequently, an increase in muscle fat fraction will result in more slowly decaying signal that results in measuring a prolonged T_2 relaxation time. This increase in the T_2 relaxation time is proportional to the fat fraction, and may falsely indicate muscle inflammation. Hence, additional approaches are necessary to separate the contribution of the fat and water protons to the total T_2 signal in order to derive the true water T_2. This is particularly important in situations where a significant amount of fat is present.

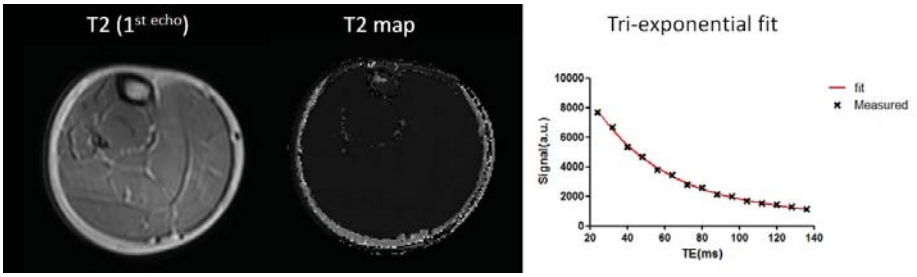

Figure 5. Axial multi-spin echo images of the right lower leg of non-fat infiltrated muscles of a DMD patient showing the 1st echo (TE: 8ms); the reconstructed T_2 map based on a tri-exponential fit; and the corresponding fit of a single point located in the Soleus muscle.

There are multiple approaches to separate the contribution of the water and fat protons. Two of these approaches are often used in skeletal muscle T_2 measurements and will be discussed in more detail. The first one is based on an addition to the acquisition scheme, a Spectrally Adiabatic Inversion Recovery (SPAIR) fat suppression pulse aimed at the main methylene and methyl fat peak.[67] (Figure 2) This resonance-specific method is based on the idea that when fully suppressing the main fat peak one can solely acquire the water signal. This method then assumes mono-exponential behavior of the water protons. It is important to note that this approach is highly sensitive to B_0 inhomogeneities as it has a resonance-specific fat suppression pulse. As a result, one should be extremely careful when using this method for quantification purposes because the fat suppression pulse can be inconsistent between examinations. In addition, previous work also showed that the significant influence of the fat signal on the measurement increased in the higher fat ranges.[68] This suggests that this measurement does not purely reflect the water signal. The second approach separates the multi-exponential behavior of the T_2 signal in post-processing by either a tri-exponential or an Extended Phase Graph (EPG) based fit. [43,69,70] A minimum number of echoes is essential to obtain a proper fit of the signal and advanced post-processing is needed to obtain quantitative values.

The MSE in combination with the advanced tri-exponential fitting method has been used in all studies assessing water T_2 in this thesis (Figure 5).

There are a few factors which need to be considered during quantification. First of all, the MSE method is more sensitive to B_1^+ field inhomogeneities compared to the MRS approach due to the larger field of view (FOV). The effect of these potential B_1^+ inhomogeneities should be taken into account when using the MSE approach. The EPG based fit incorporated these B_1^+ field fluctuations in the model, but that is not the case for the advanced tri-exponential signal fit. Consequently, in that case additional approaches, for example mapping of the B_1^+ field, are necessary to correct for these B_1^+ inhomogeneities (see the next section). Secondly, relatively high water T_2 values have been found with the advanced fit MSE approach compared to the MRS approach.[71] This difference in T_2 values has been attributed to imperfect slice profiles in the MSE approach caused by the absence of adequate RF-spoiling schemes on most clinical systems.[66,71] These RF imperfections result in stimulated echoes (additional signal) which can result in measuring elevated water T_2 values. This needs to be considered when comparing water T_2 values between studies.

1.6 B_1^+ field mapping approaches

There are two approaches often used to map the B_1^+ field: the double angle method (DAM) and the double TR method for actual flip angle imaging (AFI). [72,73] The double angle method acquires two images, one at flip angle α and one at $2*\alpha$, whereby the true flip angle can be derived from those two images by calculation. The double TR method uses two varying repetition times to derive the actual Flip Angle. This B_1^+ field information can be used as prior knowledge or as cut-off values in post-processing to ensure data-quality in any B_1^+ field sensitive acquisition. To date, this is still a relatively time-consuming process without any direct diagnostic value, so acceleration of this process is highly desirable. Recently, a relatively new fast Dual Refocusing Echo Acquisition Mode (DREAM) B_1^+ mapping technique has been proposed which allows acceleration by two orders of a magnitude. This method seems very promising but needs further evaluation in clinical applications.[74,75]

1.7 Diffusion Tensor Imaging to assess muscle structure

Diffusion Tensor Imaging (DTI) is a quantitative imaging technique aimed at probing water diffusion, the random microscopic movement of water, which in skeletal muscle is hindered by structures such as mitochondria, the sarcoplasmic reticulum, macromolecules and the cell membrane. This hindered diffusion can be described by a parameter called the apparent diffusion coefficient (ADC), which is an indirect reflection of the muscle microstructure. Introducing diffusion weighting into the

sequence attenuates the signal more from tissues which allow unrestricted diffusion of water, thus producing higher relative signals from tissues in which the movement is restricted. By using two or more diffusion-weighted sequences and comparing the relative tissue signal intensities it is possible to calculate ADC maps, showing diffusive properties of tissue in different regions of interest.

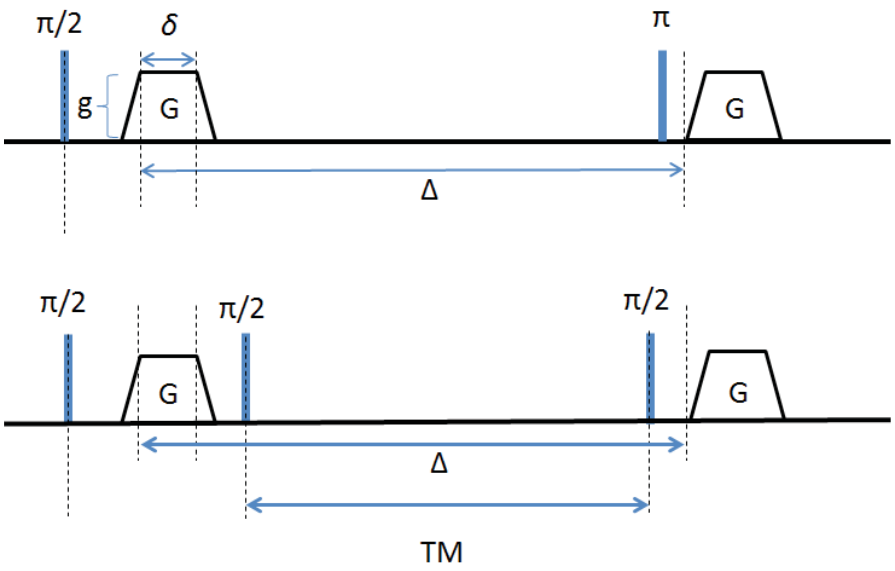

Figure 6. A schematic representation of the different diffusion modules: Spin Echo sequence (top) and a Stimulated Echo Sequence (bottom). g is the gradient amplitude, δ is the gradient duration, Δ is the spacing, and TM is the mixing time.

There are two main MR techniques used to map the diffusion properties of water in skeletal muscle. The first is the spin-echo echo-planar imaging sequence (SE-EPI), a fast, movement-robust and intrinsically T_2-weighted method, most commonly used with Stejskal-Tanner diffusion encoding (Figure 6 (top)).[76] The main challenge for this method is to achieve sufficient diffusion weighting within reasonable echo times since muscle tissue has a relatively short T_2 relaxation time. The amount of diffusion weighting is directly related to the *b*-value, a higher *b*-value generates more diffusion weighting. A given *b*-value is dependent on the gradient amplitude (g), gradient strength, the gyromagnetic ratio of the nucleus and the gradient spacing duration between the dephasing and rephrasing gradients (Δ). There are two ways to increase diffusion weighting: higher gradient strength (g) or longer gradient duration (*δ*). (Figure 6) However, the maximal gradient strength on most clinical scanners is limited due to subject safety limitations. In order to reach

higher *b*-values one has to increase the gradient spacing or duration. Both of these adjustments result in longer TE's which has a high impact on Signal to Noise Ratio (SNR) due to the muscle tissue's short T_2. An alternative approach is the Stimulated Echo (STE) sequence which avoids the T_2 decay by storing the magnetization in the longitudinal plane, which causes the signal to be attenuated by T_1 decay, and $T_1 > T_2$ for all tissues.[77] The 180-degree refocusing pulse is replaced by two 90-degree radio frequency pulses which are separated by the mixing time (TM). (Figure 6 (bottom)) This results in a direct loss of approximately 50% of the signal but allows much longer mixing times within the same echo time. These longer mixing times result in the ability to probe longer distances which can be advantageous in larger structures.

A minimum of six non-collinear diffusion directions are necessary in order to quantify the directionality of the diffusion within one individual voxel by calculating the diffusion tensor. The tensor can be diagonalized to obtain three eigenvectors (v_1, v_2, v_3) and their corresponding eigenvalues (λ_1, λ_2, λ_3). These eigenvalues are commonly used as DTI based outcome parameters. The first eigenvalue (λ_1) represents the direction in which diffusion is dominant. As such, in skeletal muscle this represents diffusion along the fiber length; the first eigenvector defines the fiber orientation with respect to the scanner coordinate system. The second eigenvalue (λ_2) points along a direction that is orthogonal to the first eigenvector (v_1). The third eigenvalue (λ_3) is orthogonal to both the first eigenvector (v_1) and the second eigenvector (v_2). If diffusion is isotropic all eigenvalues ($\lambda_1 = \lambda_2 = \lambda_3$) are equal, whereas when it is anisotropic the first eigenvalue is larger than the other two eigenvalues ($\lambda_1 > \lambda_2 = \lambda_3$ or $\lambda_1 > \lambda_2 > \lambda_3$). Radial diffusivity is the average of the second and third eigenvalue (λ_2 and λ_3) and represents the average diffusion orthogonal to the dominant direction. The radial diffusivity is thought to be most sensitive to changes in muscle due to the elongated shape of the fibers. From these three eigenvalues two other measures can be computed. The mean diffusivity (MD) is the average of the three eigenvalues and reflects the average diffusion in tissue. The fractional anisotropy (FA) is a dimensionless scalar index which varies between zero (isotropic) and one (anisotropic) and reflects the amount of directionality in the tissue. [78,79] These five measures are generally used to describe tissue microstructure and have been shown to change with respect to age, gender, exercise, injury and disease; and to vary between individual muscles.[80-94] [95]

High quality data is essential to obtain reliable estimates of these DTI-based parameters. However, reaching sufficient SNR is challenging in skeletal muscle due to the tissue's short T_2, long T_1 and relatively high diffusivity of water. Simulation studies have evaluated the effect of SNR on the DTI parameter estimation. They predicted

an underestimation of MD and the three eigenvalues, and an overestimation of FA in low SNR data.[80,89] In addition, changes in $T_{2,}$ often associated with muscle damage may indirectly influence the DTI parameter estimation in the SE-EPI sequence due to associated changes in SNR. Finally, simulation studies showed that the presence of fat signal can result in an inaccurate DTI parameter estimation due to the fact that fat has a diffusion coefficient two orders of magnitude lower than water. [96] This is particularly important in applications where there is a significant amount of fat tissue present in the region of interest, such as in muscular dystrophies. Multiple approaches have been investigated in order to suppress the effect of the fat signal.[97] One of the methods which generates good overall suppression of the spectrum is a combination of a SPAIR pulse and a Slice Selective Gradient Reversal (SSGR) technique both aimed at the main methylene and methyl fat peaks, together with a second spectral suppression pulse aimed at the olefinic fat peak. (Figure 3) Essential to keep in mind is that this method needs adjustments on the acquisition side and is highly sensitive to B_0 field inhomogeneities.[96] Recently, a relatively new method has been introduced which uses an arbitrary chemical-shift angle dual echo Dixon method to perform image reconstruction of diffusion-weighted images with suppression of the entire fat spectrum. [98] The SE-EPI sequence in combination with the three-component fat saturation technique was used for all DTI measurements in this thesis.

1.8 Phosphorous Magnetic Resonance Spectroscopy (^{31}P MRS) to assess energy metabolism

^{31}P MRS is a quantitative technique used to assess energy metabolism in skeletal muscle either in rest or in non-steady state conditions. As mentioned previously, this technique is based on the concept that nuclei of the same type, in this case ^{31}P, resonate at slightly different frequencies in different chemical environments, due to minor differences in shielding exerted by the electron cloud. This gives rise to a spectrum of frequencies which can be assigned to known metabolites. A ^{31}P spectrum of skeletal muscle contains a variety of peaks from (muscle) metabolites including Inorganic Phosphate (Pi), Phosphocreatine (PCr), Phosphodiesters (PDE), Phosphomonoesters (PME) and Adenine-Tri-Phosphate (ATP). An example of a spectrum obtained in skeletal muscle at a 7T MR system is shown in figure 7.

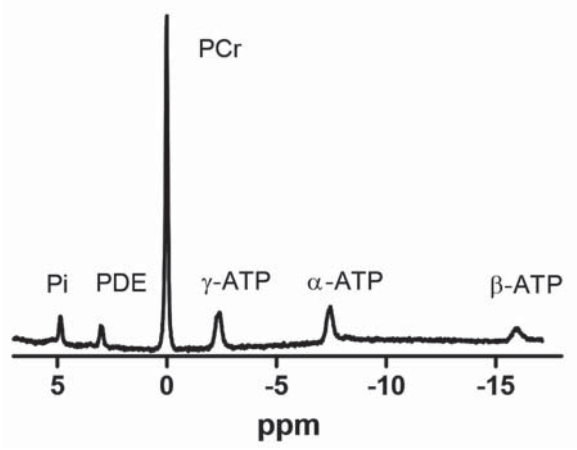

Figure. 1.7: Typical ^{31}P spectra of the Soleus muscle of a healthy (adult) control subject.

Ratios between these phosphorous compounds can reflect for instance muscle metabolic reserve and oxidative phosphorylation capacity. [99,100] In addition, the shift in resonance between the Pi and PCr peak can be used to calculate the intracellular tissue pH. These ratios and intracellular tissue pH slightly vary between the individual muscles at rest.[101,102]

MRS measurements are commonly based on a simple free induction decay (FID) readout without gradients during the spatial encoding which results in signal without any spatial information. There are three ways commonly used to spatially localize MRS data: surface coil localization, single voxel localization and spectroscopic imaging. Surface coil localization is most commonly used for ^{31}P MRS measurements in skeletal muscle and is based on measuring one single FID for all the signal picked up by the coil. This method is very fast and has short TE's which is advantageous since ^{31}P compounds have relatively short T_2 relaxation times. The sensitivity of this method is highly influenced by the shape and size of the coil, and the signal is weighted towards tissue located more closely to the surface. Consequently, the signal obtained with this method is a mixture of multiple tissue types and has a high inter-subject variability which needs to be considered when interpreting the results. Secondly, there are single-voxel localization approaches which generate rapid information from a well-defined small ROI with a relatively homogeneous magnetic field. This method uses a combination of three slice-selective RF pulses in orthogonal planes through which a signal arises at the intersection of these three planes. This localization method is highly sensitive to the chemical shift displacement artefact (CSDA), especially at high magnetic fields, and works less efficiently in heterogeneous tissue types. In addition, the relatively long TE's, pertinent to this

method, in combination with the relatively short T_2 times of the various phosphorous compounds result in a lot of signal loss. [103] Lastly, there are Chemical Shift Imaging (CSI) methods which became increasingly more popular with the availability of higher field magnets. The acquisition of this technique is based on a simple FID readout, spatially localized in 1D, 2D or 3D by a combination of a single excitation pulse and phase encoding steps. This technique is very well suited for heterogeneous tissue types, is relatively efficient in terms of SNR per unit of time but has long acquisition times and less well-defined voxels. Besides spectroscopy, one could also use spectrally sensitive ^{31}P imaging. This imaging technique can be used to map PCr with high temporal and spatial resolution compared to spectroscopy approaches. This is advantageous in exercise settings and heterogeneous tissue types. However, this method is only aimed at one or two resonances, which limits application possibilities.[104] The 2D chemical shift imaging method was used for all ^{31}P MRS studies in this thesis.

There are a few general points which need to be considered when quantitatively assessing energy metabolism with ^{31}P MRS. First, one of the most essential points for MRS in general is adequate shimming of the B_0 field which has a direct relation to SNR and linewidth. Generally, a drop in SNR and an increase in linewidth result in a less accurate estimation of the area under curve and thus of the metabolite ratios. These effects can be minimized by enforcing strict acceptance criteria that limit spectra to minimum SNR and maximum linewidths to ensure proper quantification and comparisons of energy metabolism among individuals. Second, the saturation effect due to variation in T_1 relaxation of the various phosphorus compounds needs to be considered. In practice, the T_1 relaxation times of ^{31}P metabolites are too long to allow complete saturation before the next excitation pulse. These relaxation effects can be accounted for in post-processing using literature values, or by measuring the full relaxation of the various compounds. They can also be reduced during acquisition by using the Ernst angle for excitation. [103] Last, all individual phosphorous compounds are generally presented as a ratio over β-ATP. This quantification method assumes that muscle ATP is constant or at least is preserved as long as possible in skeletal muscle. However, this might not always be the case.

1.9 Objectives of this thesis

The overall aim of this thesis was to combine various quantitative MR measurements and to compare these between DMD patients and healthy age-matched controls, both on a cross-sectional and longitudinal level, to generate a better understanding of the underlying pathophysiology and ideally to explore the value of these MR outcome parameters to monitor muscle tissue changes in a clinical setting. In order to achieve this aim we:

1. measured muscle fat infiltration, inflammation, fiber architecture and energy metabolism in healthy and diseased muscle on a cross-sectional and longitudinal level.
2. combined these MR techniques to assess the effect of spatial localization, data quality and confounding factors on the quantification process of MR outcome measures.
3. combined these MR parameters to have a better understanding of the underlying pathophysiology of DMD.

Thesis Outline

This thesis is divided into two main parts, preceded by an introduction and followed by a general discussion. The first part focuses on the effect of methodological factors such as data-quality, accurate spatial localization and confounding factors on quantification of MR outcome measures in skeletal muscle applications. In chapter 2, the effect of %fat, SNR and T_2 changes on the DTI measurements in skeletal muscle of DMD patients and healthy controls has been evaluated using multi-parametric MRI. In chapter 3, the accuracy of spatial localization is stressed using 3-point-dixon imaging for fat quantification along the proximodistal muscle axis in DMD patients. In chapter 5, the effect of data quality, accuracy and reproducibility of quantifying PDE-levels with ^{31}P MRS was assessed in healthy control subjects. The second part of this thesis is focused on the importance of combining various imaging techniques in order to have a better understanding of the underlying pathophysiology in DMD and to explore the value of MR measures to monitor muscle tissue changes. Chapter 3 assessed variations in muscle degeneration within individual leg muscles of DMD patients. Chapter 4 presents combined qMRI and spatially-resolved (2D-CSI) ^{31}P MRS data of the leg muscles in DMD patients to determine metabolic changes and inflammation in muscles with and without fat infiltration, to assess if metabolic changes and inflammation vary in different stages of the disease process. Chapter 5 presents longitudinal and spatially resolved ^{31}P MRS and qMRI data of lower leg muscles that represent varying levels of muscle deterioration, aimed to assess whether phosphodiester (PDE)-levels detected by ^{31}P MRS could be a marker for muscle tissue changes. In addition, the course of the other metabolic indices over two-year time-period was assessed. Finally, chapter 6 aims to bridge the gap between the research field and clinical practice by accelerating of sequences, as it focuses on the implementation of a fast B_1^+ shimming technique to improve image quality, in whole body imaging at 3T, without loss of essential scan time.

1.10 References

1 Ryder, S. *et al.* The burden, epidemiology, costs and treatment for Duchenne muscular dystrophy: an evidence review. *Orphanet J Rare Dis* **12**, 79, doi:10.1186/s13023-017-0631-3 (2017).

2 Hoffman, E. P., Brown, R. H. & Kunkel, L. M. Dystrophin - the Protein Product of the Duchenne Muscular-Dystrophy Locus. *Cell* **51**, 919-928, doi:Doi 10.1016/0092-8674(87)90579-4 (1987).

3 Jennekens, F. G., ten Kate, L. P., de Visser, M. & Wintzen, A. R. Diagnostic criteria for Duchenne and Becker muscular dystrophy and myotonic dystrophy. *Neuromuscul Disord* **1**, 389-391 (1991).

4 Blake, D. J., Weir, A., Newey, S. E. & Davies, K. E. Function and genetics of dystrophin and dystrophin-related proteins in muscle. *Physiol Rev* **82**, 291-329, doi:10.1152/physrev.00028.2001 (2002).

5 Kinali, M. *et al.* Muscle histology vs MRI in Duchenne muscular dystrophy. *Neurology* **76**, 346-353, doi:Doi 10.1212/Wnl.0b013e318208811f (2011).

6 Eagle, M. *et al.* Managing Duchenne muscular dystrophy--the additive effect of spinal surgery and home nocturnal ventilation in improving survival. *Neuromuscul Disord* **17**, 470-475, doi:10.1016/j.nmd.2007.03.002 (2007).

7 Ishikawa, Y. *et al.* Duchenne muscular dystrophy: survival by cardio-respiratory interventions. *Neuromuscul Disord* **21**, 47-51, doi:10.1016/j.nmd.2010.09.006 (2011).

8 Eagle, M. *et al.* Survival in Duchenne muscular dystrophy: improvements in life expectancy since 1967 and the impact of home nocturnal ventilation. *Neuromuscul Disord* **12**, 926-929 (2002).

9 Nigro, G., Comi, L. I., Politano, L. & Bain, R. J. The incidence and evolution of cardiomyopathy in Duchenne muscular dystrophy. *Int J Cardiol* **26**, 271-277 (1990).

10 Cotton, S. M., Voudouris, N. J. & Greenwood, K. M. Association between intellectual functioning and age in children and young adults with Duchenne muscular dystrophy: further results from a meta-analysis. *Dev Med Child Neurol* **47**, 257-265 (2005).

11 Mehler, M. F. Brain dystrophin, neurogenetics and mental retardation. *Brain Res Brain Res Rev* **32**, 277-307 (2000).

12 Cyrulnik, S. E., Fee, R. J., De Vivo, D. C., Goldstein, E. & Hinton, V. J. Delayed developmental language milestones in children with Duchenne's muscular dystrophy. *J Pediatr* **150**, 474-478, doi:10.1016/j.jpeds.2006.12.045 (2007).

13 Kieny, P. *et al.* Evolution of life expectancy of patients with Duchenne muscular dystrophy at AFM Yolaine de Kepper centre between 1981 and 2011. *Ann Phys Rehabil Med* **56**, 443-454, doi:10.1016/j.rehab.2013.06.002 (2013).

14 Ervasti, J. M., Ohlendieck, K., Kahl, S. D., Gaver, M. G. & Campbell, K. P. Deficiency of a glycoprotein component of the dystrophin complex in dystrophic muscle. *Nature* **345**, 315-319, doi:10.1038/345315a0 (1990).

15 Rybakova, I. N., Patel, J. R. & Ervasti, J. M. The dystrophin complex forms a mechanically strong link between the sarcolemma and costameric actin. *J Cell Biol* **150**, 1209-1214, doi:DOI 10.1083/jcb.150.5.1209 (2000).

16 Allen, D. G., Whitehead, N. P. & Froehner, S. C. Absence of Dystrophin Disrupts Skeletal Muscle Signaling: Roles of Ca2+, Reactive Oxygen Species, and Nitric Oxide in the Development of Muscular Dystrophy. *Physiol Rev* **96**, 253-305, doi:10.1152/physrev.00007.2015 (2016).

17 Peverelli, L. *et al.* Histologic muscular history in steroid-treated and untreated patients with Duchenne dystrophy. *Neurology* **85**, 1886-1893, doi:10.1212/Wnl.0000000000002147 (2015).

18 Deconinck, N. & Dan, B. Pathophysiology of duchenne muscular dystrophy: current hypotheses. *Pediatr Neurol* **36**, 1-7, doi:10.1016/j.pediatrneurol.2006.09.016 (2007).

19 Bell, C. D. & Conen, P. E. Histopathological changes in Duchenne muscular dystrophy. *J Neurol Sci* **7**, 529-544 (1968).

20 Wokke, B. H. *et al.* Quantitative MRI and strength measurements in the assessment of muscle quality in Duchenne muscular dystrophy. *Neuromuscular Disord* **24,** 409-416, doi:10.1016/j.nmd.2014.01.015 (2014).

21 Karpati, G., Carpenter, S. & Prescott, S. Small-caliber skeletal muscle fibers do not suffer necrosis in mdx mouse dystrophy. *Muscle Nerve* **11,** 795-803, doi:10.1002/mus.880110802 (1988).

22 Straub, V. *et al.* Stakeholder cooperation to overcome challenges in orphan medicine development: the example of Duchenne muscular dystrophy. *Lancet Neurol* **15,** 882-890 (2016).

23 Fischmann, A. *et al.* Muscular involvement assessed by MRI correlates to motor function measurement values in oculopharyngeal muscular dystrophy. *J Neurol* **258,** 1333-1340, doi:10.1007/s00415-011-5937-9 (2011).

24 Fischmann, A. *et al.* Quantitative MRI can detect subclinical disease progression in muscular dystrophy. *J Neurol* **259,** 1648-1654, doi:10.1007/s00415-011-6393-2 (2012).

25 Fischmann, A. *et al.* Quantitative MRI and loss of free ambulation in Duchenne muscular dystrophy. *J Neurol* **260,** 969-974, doi:10.1007/s00415-012-6733-x (2013).

26 Hollingsworth, K. G., Garrood, P., Eagle, M., Bushby, K. & Straub, V. Magnetic Resonance Imaging in Duchenne Muscular Dystrophy: Longitudinal Assessment of Natural History over 18 Months. *Muscle Nerve* **48,** 586-588, doi:10.1002/mus.23879 (2013).

27 Ricotti, V. *et al.* Upper Limb Evaluation in Duchenne Muscular Dystrophy: Fat-Water Quantification by MRI, Muscle Force and Function Define Endpoints for Clinical Trials. *Plos One* **11,** e0162542, doi:10.1371/journal.pone.0162542 (2016).

28 Bonati, U. *et al.* Quantitative muscle MRI: A powerful surrogate outcome measure in Duchenne muscular dystrophy. *Neuromuscul Disord* **25,** 679-685, doi:10.1016/j.nmd.2015.05.006 (2015).

29 Wren, T. A., Bluml, S., Tseng-Ong, L. & Gilsanz, V. Three-point technique of fat quantification of muscle tissue as a marker of disease progression in Duchenne muscular dystrophy: preliminary study. *AJR Am J Roentgenol* **190,** W8-12, doi:10.2214/AJR.07.2732 (2008).

30 Willcocks, R. J. *et al.* Longitudinal measurements of MRI-T-2 in boys with Duchenne muscular dystrophy: Effects of age and disease progression. *Neuromuscular Disord* **24,** 393-401, doi:10.1016/j.nmd.2013.12.012 (2014).

31 Arpan, I. *et al.* T-2 mapping provides multiple approaches for the characterization of muscle involvement in neuromuscular diseases: a cross-sectional study of lower leg muscles in 5-15-year-old boys with Duchenne muscular dystrophy. *Nmr Biomed* **26,** 320-328, doi:10.1002/nbm.2851 (2013).

32 Forbes, S. C. *et al.* Magnetic Resonance Imaging and Spectroscopy Assessment of Lower Extremity Skeletal Muscles in Boys with Duchenne Muscular Dystrophy: A Multicenter Cross Sectional Study. *Plos One* **9,** doi:ARTN e106435
10.1371/journal.pone.0106435 (2014).

33 Arpan, I. *et al.* Examination of effects of corticosteroids on skeletal muscles of boys with DMD using MRI and MRS. *Neurology* **83,** 974-980, doi:10.1212/WNL.0000000000000775 (2014).

34 Kemp, G. J., Taylor, D. J., Dunn, J. F., Frostick, S. P. & Radda, G. K. Cellular Energetics of Dystrophic Muscle. *J Neurol Sci* **116,** 201-206, doi:Doi 10.1016/0022-510x(93)90326-T (1993).

35 Griffiths, R. D., Cady, E. B., Edwards, R. H. & Wilkie, D. R. Muscle energy metabolism in Duchenne dystrophy studied by 31P-NMR: controlled trials show no effect of allopurinol or ribose. *Muscle Nerve* **8,** 760-767, doi:10.1002/mus.880080904 (1985).

36 Newman, R. J. *et al.* Nuclear Magnetic-Resonance Studies of Forearm Muscle in Duchenne Dystrophy. *Brit Med J* **284,** 1072-1074 (1982).

37 Younkin, D. P. *et al.* 31P NMR studies in Duchenne muscular dystrophy: age-related metabolic changes. *Neurology* **37,** 165-169 (1987).

38 Hogrel, J. Y. *et al.* Longitudinal functional and NMR assessment of upper limbs in Duchenne muscular dystrophy. *Neurology* **86,** 1022-1030, doi:10.1212/Wnl.0000000000002464 (2016).

39 Wary, C. *et al.* Quantitative NMRI and NMRS identify augmented disease progression after loss of ambulation in forearms of boys with Duchenne muscular dystrophy. *Nmr Biomed* **28**, 1150-1162, doi:10.1002/nbm.3352 (2015).

40 Wary, C. *et al.* Nuclear Magnetic Resonance imaging and spectroscopy provide quantitative indices of disease severity in forearms of boys with Duchenne Muscle Dystrophy. *Neuromuscular Disord* **23**, 810-810, doi:10.1016/j.nmd.2013.06.600 (2013).

41 Wary, C. *et al.* One year follow-up of Duchenne muscle dystrophy with nuclear magnetic resonance imaging and spectroscopy indices. *Neuromuscular Disord* **24**, 853-853, doi:10.1016/j.nmd.2014.06.201 (2014).

42 de Amorim e Silva, C. J., Mackenzie, A., Hallowell, L. M., Stewart, S. E. & Ditchfield, M. R. Practice MRI: reducing the need for sedation and general anaesthesia in children undergoing MRI. *Australas Radiol* **50**, 319-323, doi:10.1111/j.1440-1673.2006.01590.x (2006).

43 Azzabou, N., Loureiro de Sousa, P., Caldas, E. & Carlier, P. G. Validation of a generic approach to muscle water T2 determination at 3T in fat-infiltrated skeletal muscle. *J Magn Reson Imaging* **41**, 645-653, doi:10.1002/jmri.24613 (2015).

44 Janssen, B., Voet, N., Geurts, A., van Engelen, B. & Heerschap, A. Quantitative MRI reveals decelerated fatty infiltration in muscles of active FSHD patients. *Neurology* **86**, 1700-1707, doi:10.1212/WNL.0000000000002640 (2016).

45 Choi, S. J. *et al.* Intramyocellular Lipid and Impaired Myofiber Contraction in Normal Weight and Obese Older Adults. *J Gerontol A Biol Sci Med Sci* **71**, 557-564, doi:10.1093/gerona/glv169 (2016).

46 Son, J. W. *et al.* Low muscle mass and risk of type 2 diabetes in middle-aged and older adults: findings from the KoGES. *Diabetologia*, doi:10.1007/s00125-016-4196-9 (2017).

47 Reeder, S. B. *et al.* Quantification of hepatic steatosis with MRI: the effects of accurate fat spectral modeling. *J Magn Reson Imaging* **29**, 1332-1339, doi:10.1002/jmri.21751 (2009).

48 Dixon, W. T. Simple proton spectroscopic imaging. *Radiology* **153**, 189-194, doi:10.1148/radiology.153.1.6089263 (1984).

49 Glover, G. H. & Schneider, E. Three-point Dixon technique for true water/fat decomposition with Bo inhomogeneity correction. *Magn Reson Med* **18**, 371-383 (1991).

50 Kuroda, K., Oshio, K., Mulkern, R. V. & Jolesz, F. A. Optimization of chemical shift selective suppression of fat. *Magn Reson Med* **40**, 505-510 (1998).

51 Hernando, D., Kellman, P., Haldar, J. P. & Liang, Z. P. Robust water/fat separation in the presence of large field inhomogeneities using a graph cut algorithm. *Magn Reson Med* **63**, 79-90, doi:10.1002/mrm.22177 (2010).

52 Hu, H. H. *et al.* ISMRM workshop on fat-water separation: insights, applications and progress in MRI. *Magn Reson Med* **68**, 378-388, doi:10.1002/mrm.24369 (2012).

53 Liu, C. Y., McKenzie, C. A., Yu, H., Brittain, J. H. & Reeder, S. B. Fat quantification with IDEAL gradient echo imaging: correction of bias from T(1) and noise. *Magn Reson Med* **58**, 354-364, doi:10.1002/mrm.21301 (2007).

54 Bydder, M. *et al.* Relaxation effects in the quantification of fat using gradient echo imaging. *Magn Reson Imaging* **26**, 347-359, doi:10.1016/j.mri.2007.08.012 (2008).

55 Reeder, S. B. *et al.* Water-fat separation with IDEAL gradient-echo imaging. *J Magn Reson Imaging* **25**, 644-652, doi:10.1002/jmri.20831 (2007).

56 Wokke, B. H. *et al.* Comparison of dixon and T1-weighted MR methods to assess the degree of fat infiltration in duchenne muscular dystrophy patients. *J Magn Reson Imaging* **38**, 619-624, doi:10.1002/jmri.23998 (2013).

57 Yu, H. Z. *et al.* Multiecho Water-Fat Separation and Simultaneous R-2* Estimation With Multifrequency Fat Spectrum Modeling. *Magn Reson Med* **60**, 1122-1134, doi:10.1002/mrm.21737 (2008).

58 Loughran, T. *et al.* Improving Highly Accelerated Fat Fraction Measurements for Clinical Trials in Muscular Dystrophy: Origin and Quantitative Effect of R2*Changes. *Radiology* **275**, 570-578, doi:10.1148/radiol.14141191 (2015).

59 Araujo, E. C., Fromes, Y. & Carlier, P. G. New insights on human skeletal muscle tissue compartments revealed by in vivo t2 NMR relaxometry. *Biophys J* **106**, 2267-2274, doi:10.1016/j.bpj.2014.04.010 (2014).

60 McCully, K. & Posner, J. Measuring exercise-induced adaptations and injury with magnetic resonance spectroscopy. *Int J Sports Med* **13 Suppl 1**, S147-149, doi:10.1055/s-2007-1024621 (1992).

61 Damon, B. M. *et al.* Intracellular acidification and volume increases explain R(2) decreases in exercising muscle. *Magn Reson Med* **47**, 14-23 (2002).

62 Arpan, I. *et al.* Examination of effects of corticosteroids on skeletal muscles of boys with DMD using MRI and MRS. *Neurology* **83**, 974-980 (2014).

63 Willcocks, R. J. *et al.* Longitudinal measurements of MRI-T2 in boys with Duchenne muscular dystrophy: effects of age and disease progression. *Neuromuscul Disord* **24**, 393-401, doi:10.1016/j.nmd.2013.12.012 (2014).

64 Willcocks, R. J. *et al.* Magnetic resonance imaging and spectroscopy detect changes with age, corticosteroid treatment, and functional progression in DMD. *Neuromuscular Disord* **23**, 810-810, doi:10.1016/j.nmd.2013.06.599 (2013).

65 Fullerton, G. D., Cameron, I. L., Hunter, K. & Fullerton, H. J. Proton magnetic resonance relaxation behavior of whole muscle with fatty inclusions. *Radiology* **155**, 727-730, doi:10.1148/radiology.155.3.4001376 (1985).

66 Carlier, P. G. Global T2 versus water T2 in NMR imaging of fatty infiltrated muscles: Different methodology, different information and different implications. *Neuromuscular Disord* **24**, 390-392, doi:10.1016/j.nmd.2014.02.009 (2014).

67 Bley, T. A., Wieben, O., Francois, C. J., Brittain, J. H. & Reeder, S. B. Fat and water magnetic resonance imaging. *J Magn Reson Imaging* **31**, 4-18, doi:10.1002/jmri.21895 (2010).

68 Wokke, B. H. *et al.* T2 relaxation times are increased in Skeletal muscle of DMD but not BMD patients. *Muscle Nerve* **53**, 38-43, doi:10.1002/mus.24679 (2016).

69 Lebel, R. M. & Wilman, A. H. Transverse relaxometry with stimulated echo compensation. *Magn Reson Med* **64**, 1005-1014, doi:10.1002/mrm.22487 (2010).

70 Marty, B. *et al.* Simultaneous muscle water T2 and fat fraction mapping using transverse relaxometry with stimulated echo compensation. *Nmr Biomed* **29**, 431-443, doi:10.1002/nbm.3459 (2016).

71 Forbes, S. C. *et al.* Skeletal Muscles of Ambulant Children with Duchenne Muscular Dystrophy: Validation of Multicenter Study of Evaluation with MR Imaging and MR Spectroscopy. *Radiology* **269**, 198-207, doi:10.1148/radiol.13121948 (2013).

72 Stollberger, R. & Wach, P. Imaging of the active B1 field in vivo. *Magn Reson Med* **35**, 246-251 (1996).

73 Yarnykh, V. L. Actual flip-angle imaging in the pulsed steady state: a method for rapid three-dimensional mapping of the transmitted radiofrequency field. *Magn Reson Med* **57**, 192-200, doi:10.1002/mrm.21120 (2007).

74 Nehrke, K. & Bornert, P. DREAM--a novel approach for robust, ultrafast, multislice B(1) mapping. *Magn Reson Med* **68**, 1517-1526, doi:10.1002/mrm.24158 (2012).

75 Sacolick, L. I., Wiesinger, F., Hancu, I. & Vogel, M. W. B1 mapping by Bloch-Siegert shift. *Magn Reson Med* **63**, 1315-1322, doi:10.1002/mrm.22357 (2010).

76 Steidle, G. & Schick, F. Echoplanar diffusion tensor imaging of the lower leg musculature using eddy current nulled stimulated echo preparation. *Magn Reson Med* **55**, 541-548, doi:10.1002/mrm.20780 (2006).

77 Karampinos, D. C., Banerjee, S., King, K. F., Link, T. M. & Majumdar, S. Considerations in high-resolution skeletal muscle diffusion tensor imaging using single-shot echo planar imaging with stimulated-echo preparation and sensitivity encoding. *Nmr Biomed* **25**, 766-778, doi:10.1002/nbm.1791 (2012).

78 Basser, P. J. & Pierpaoli, C. Microstructural and physiological features of tissues elucidated by quantitative-diffusion-tensor MRI. *J Magn Reson B* **111**, 209-219 (1996).

79 Pierpaoli, C. & Basser, P. J. Toward a quantitative assessment of diffusion anisotropy. *Magn Reson Med* **36**, 893-906 (1996).

80 Damon, B. M. Effects of image noise in muscle diffusion tensor (DT)-MRI assessed using numerical simulations. *Magn Reson Med* **60**, 934-944, doi:10.1002/mrm.21707 (2008).

81 Damon, B. M., Ding, Z., Anderson, A. W., Freyer, A. S. & Gore, J. C. Validation of diffusion tensor MRI-based muscle fiber tracking. *Magn Reson Med* **48**, 97-104, doi:10.1002/mrm.10198 (2002).

82 Damon, B. M., Heemskerk, A. M. & Ding, Z. Polynomial fitting of DT-MRI fiber tracts allows accurate estimation of muscle architectural parameters. *Magn Reson Imaging* **30**, 589-600, doi:10.1016/j.mri.2012.02.003 (2012).

83 Zaraiskaya, T., Kumbhare, D. & Noseworthy, M. D. Diffusion tensor imaging in evaluation of human skeletal muscle injury. *J Magn Reson Imaging* **24**, 402-408, doi:10.1002/jmri.20651 (2006).

84 Qi, J., Olsen, N. J., Price, R. R., Winston, J. A. & Park, J. H. Diffusion-weighted imaging of inflammatory myopathies: polymyositis and dermatomyositis. *J Magn Reson Imaging* **27**, 212-217, doi:10.1002/jmri.21209 (2008).

85 Galban, C. J., Maderwald, S., Uffmann, K. & Ladd, M. E. A diffusion tensor imaging analysis of gender differences in water diffusivity within human skeletal muscle. *Nmr Biomed* **18**, 489-498, doi:10.1002/nbm.975 (2005).

86 Budzik, J. F. *et al.* In vivo MR tractography of thigh muscles using diffusion imaging: initial results. *Eur Radiol* **17**, 3079-3085, doi:10.1007/s00330-007-0713-z (2007).

87 Heemskerk, A. M. & Damon, B. M. Diffusion Tensor MRI Assessment of Skeletal Muscle Architecture. *Curr Med Imaging Rev* **3**, 152-160, doi:10.2174/157340507781386988 (2007).

88 Heemskerk, A. M., Strijkers, G. J., Drost, M. R., van Bochove, G. S. & Nicolay, K. Skeletal muscle degeneration and regeneration after femoral artery ligation in mice: monitoring with diffusion MR imaging. *Radiology* **243**, 413-421, doi:10.1148/radiol.2432060491 (2007).

89 Froeling, M., Nederveen, A. J., Nicolay, K. & Strijkers, G. J. DTI of human skeletal muscle: the effects of diffusion encoding parameters, signal-to-noise ratio and T2 on tensor indices and fiber tracts. *Nmr Biomed* **26**, 1339-1352, doi:10.1002/nbm.2959 (2013).

90 Froeling, M. *et al.* Muscle changes detected with diffusion-tensor imaging after long-distance running. *Radiology* **274**, 548-562, doi:10.1148/radiol.14140702 (2015).

91 Froeling, M. *et al.* Reproducibility of diffusion tensor imaging in human forearm muscles at 3.0 T in a clinical setting. *Magn Reson Med* **64**, 1182-1190, doi:10.1002/mrm.22477 (2010).

92 Oudeman, J. *et al.* Techniques and applications of skeletal muscle diffusion tensor imaging: A review. *J Magn Reson Imaging* **43**, 773-788, doi:10.1002/jmri.25016 (2016).

93 Schlaffke, L. *et al.* Diffusion tensor imaging of the human calf: Variation of inter- and intramuscle-specific diffusion parameters. *J Magn Reson Imaging*, doi:10.1002/jmri.25650 (2017).

94 Scheel, M. *et al.* Diffusion tensor imaging of skeletal muscle--correlation of fractional anisotropy to muscle power. *Rofo* **185**, 857-861, doi:10.1055/s-0033-1335911 (2013).

95 Sinha, S., Sinha, U. & Edgerton, V. R. In vivo diffusion tensor imaging of the human calf muscle. *J Magn Reson Imaging* **24**, 182-190, doi:10.1002/jmri.20593 (2006).

96 Williams, S. E. *et al.* Quantitative effects of inclusion of fat on muscle diffusion tensor MRI measurements. *J Magn Reson Imaging* **38**, 1292-1297, doi:10.1002/jmri.24045 (2013).

97 Hernando, D. *et al.* Removal of olefinic fat chemical shift artifact in diffusion MRI. *Magn Reson Med* **65**, 692-701, doi:10.1002/mrm.22670 (2011).

98 Burakiewicz, J. *et al.* Improved olefinic fat suppression in skeletal muscle DTI using a magnitude-based dixon method. *Magn Reson Med*, doi:10.1002/mrm.26655 (2017).

99 Taylor, D. J., Bore, P. J., Styles, P., Gadian, D. G. & Radda, G. K. Bioenergetics of intact human muscle. A 31P nuclear magnetic resonance study. *Mol Biol Med* **1**, 77-94 (1983).

100 Prompers, J. J. *et al.* Dynamic MRS and MRI of skeletal muscle function and biomechanics. *Nmr Biomed* **19,** 927-953, doi:10.1002/nbm.1095 (2006).
101 Meyerspeer, M. *et al.* Direct noninvasive quantification of lactate and high energy phosphates simultaneously in exercising human skeletal muscle by localized magnetic resonance spectroscopy. *Magn Reson Med* **57,** 654-660, doi:10.1002/mrm.21188 (2007).
102 Vandenborne, K. *et al.* Metabolic heterogeneity in human calf muscle during maximal exercise. *Proc Natl Acad Sci U S A* **88,** 5714-5718 (1991).
103 Bogner, W. *et al.* Assessment of (31)P Relaxation Times in the Human Calf Muscle: A Comparison between 3 T and 7 T In Vivo. *Magn Reson Med* **62,** 574-582, doi:10.1002/mrm.22057 (2009).
104 Parasoglou, P., Feng, L., Xia, D., Otazo, R. & Regatte, R. R. Rapid 3D-imaging of phosphocreatine recovery kinetics in the human lower leg muscles with compressed sensing. *Magn Reson Med* **68,** 1738-1746, doi:10.1002/mrm.24484 (2012).

1